Rayleigh-Taylor convective dissolution in confined porous media

Marco De Paoli,[1,*] Francesco Zonta,[1,†] and Alfredo Soldati[1,2,‡]

[1]*Institute of Fluid Mechanics and Heat Transfer, TU Wien, 1060 Vienna, Austria*
[2]*Polytechnic Department, University of Udine, 33100 Udine, Italy*

Numerical simulations are used here to analyze the Rayleigh-Taylor instability in confined and isotropic porous media. The Rayleigh-Taylor instability phenomena arise when a layer of heavy fluid sits on top of a layer of a lighter fluid. Small fluctuations of the interface separating the two fluid layers produce larger structures that eventually drive the flow into a nonlinear convective stage. The flow is initially controlled by diffusion, but rather quickly the action of gravity produces efficient fluid mixing in the entire domain. The single parameter controlling the flow is the Rayleigh number, which is the dimensionless ratio of diffusive to convective timescales. The flow evolution is often parametrized by the mixing length (a suitably defined extension of the mixing region), which, according to Gopalakrishnan *et al.* [Phys. Rev. Fluids **2**, 012501(R) (2017)], has a linear growth. From the analysis of a broad range of simulations spanning three orders of magnitude of the Rayleigh number, we could observe a superlinear asymptotic growth of the mixing length. The present results, which are in line with previous simulations, allow us to evaluate precisely the superlinear evolution coefficient. We further provide simple scaling arguments to justify the observed superlinear growth.

I. INTRODUCTION

When a layer of heavier fluid sits on top of a layer of lighter fluid, the interface separating the two layers is prone to undergoing the Rayleigh-Taylor (RT) instability [1–3]. Gravity amplifies initially small interfacial perturbations, which possibly evolve into fingerlike structures [4]. Reportedly, the evolution of the average finger length with time is linear [5] and corresponds to a strong convective mixing of the two fluids. Both finger structures and convective mixing have been broadly investigated, with the theoretical foundations of the problem for the general case of buoyancy-driven convection in pure fluids (i.e., not restricted to the case of flows in porous media) being originally set by Rayleigh [1] and Taylor [2]. Such foundations were only later extended to the case of porous media by Saffman and Taylor [3], who derived the conditions for the stability of two immiscible fluids with different density and viscosity in a porous medium. They also introduced the idea that the flow inside a porous medium can be experimentally reproduced employing the Hele-Shaw cell, i.e., a cell composed of two large parallel plates separated by an extremely narrow size gap, which has served the purpose of many important experimental investigations [6–9]. Although obtained for the case of two immiscible fluids, the main findings of Saffman and Taylor [3] remain valid also for the case of miscible fluids considered here (see also [4] for a broader discussion of the topic). A comprehensive analysis of gravitationally unstable miscible fluids was conducted a few years later by Wooding [10], who performed experiments in a Hele-Shaw cell and found that the

---

*marco.de.paoli@tuwien.ac.at

†francesco.zonta@tuwien.ac.at

‡Author to whom correspondence should be addressed: alfredo.soldati@tuwien.ac.at

mean amplitude of fingers generated at the liquid-liquid interface grows in time as t, while their mean wavelength grows as $t^{1/2}$. A further extension of these findings, so as to cover a wider range of the governing parameters, was recently provided by [11–13] using numerical simulations. It is now widely accepted that the time behavior of fingers is related to the influence of convection and diffusion [5,14]: Convection dominates the dynamics of finger tips (hence influencing the fingers amplitude), while diffusion dominates the lateral finger spreading (hence influencing the finger width or wavelength).

It is worth noting that the problem of buoyancy-driven convection in fluid-saturated porous media has been receiving increasing attention because of its importance in a number of industrial [15,16] and environmental [17–19] applications. Specifically, the strategic planning regarding carbon dioxide (CO_2) sequestration into brine-filled geological formations has driven a number of recent works on the topic [12,20–26]. In most cases, such works envision the process of dissolution-driven CO_2 transport as a Rayleigh-Bénard-like (RB) convection. In the RB case, the solute concentration is kept constant at the top boundary. In the RT case, a lump of heavier fluid fills the top part of the domain and penetrates the lighter fluid underneath [27,28].

Theories, experiments, and simulations have recently developed a fairly robust picture of the RT instability in porous media, also providing a suitable scientific foundation for addressing more complex problems of paramount importance [for example, the inclusion of chemical reactions occurring during the fluid mixing (see [29–32])], but several aspects still remain to be fully investigated. One of these aspects is the influence of top and bottom horizontal impermeable boundaries on the overall dynamics of the flow triggered by the RT instability, and the corresponding parametrization and modeling of the entire process. This is exactly the aim of the present paper. We consider the RT instability developing in a porous medium delimited by two horizontal impermeable boundaries. The governing dimensionless parameter of the flow evolution in this case is the Rayleigh-Darcy number Ra, which represents a measure of the relative importance of buoyancy compared to diffusion in a porous medium. For small values of Ra [typically Ra $< O(10)$] fingers do not appear and the problem is fully controlled by diffusion. For larger Ra [typically Ra $> O(10^2)$], although the stretching of the fingers is dominated by convection, molecular diffusion still plays a role promoting the mixing of the two species all along the interface of the fingers (we refer the reader to [11,33,34] for further details on the stability analysis in different flow configurations).

In the present study, we use numerical simulations to perform a systematic study for a wide range of Ra so as to provide insights into the dissolution-driven convection.[1] Together with the phenomenological description of the flow structure, we will also present specific measurements of global transfer coefficients and propose reliable parametrizations and models of the process.

II. METHODOLOGY

We consider a two-dimensional homogeneous and isotropic porous domain characterized by uniform permeability k and porosity ϕ. The domain has dimensions L^* and H^* along the horizontal (x^*) and vertical (z^*) directions, respectively. The upper (lower) half of the porous domain is initially filled with a heavy (light) fluid.

In this physical configuration, the flow is driven by the composition-induced density difference in the vertical direction (where the acceleration due to gravity g is directed). The fluid motion is described by Darcy's law written in the framework of the Oberbeck-Boussinesq approximation [35]

$$\frac{\partial u^*}{\partial x^*} + \frac{\partial w^*}{\partial z^*} = 0,$$ (1)

$$\frac{\mu}{k} u^* = -\frac{\partial p^*}{\partial x^*}, \quad \frac{\mu}{k} w^* = -\frac{\partial p^*}{\partial z^*} - \rho^* g,$$ (2)

---

[1]The computational results presented have been achieved using the Vienna Scientific Cluster.

where u^* and w^* are the horizontal and vertical components of the fluid velocity, while p^* and ρ^* are pressure and density. Note that the Oberbeck-Boussinesq approximation is valid only if density variations are small compared to the reference fluid density. In many situations of practical interest, and also in the context of geophysical and environmental applications, this approximation is physically sound [19] and the adoption of the fully compressible approach does not introduce substantial changes [36]. In the present study we assume that the density of the mixture is a linear function of solute concentration C^*,

$$\rho^* = \rho_s^* \left[1 - \frac{\Delta \rho_s^*}{\rho_s^* C_s^*} (C_s^* - C^*) \right], \tag{3}$$

where ρ_s^* is the density of the dense layer of saturated fluid, C_s^* is the corresponding concentration of solute, and $\Delta \rho_s^*$ is the density difference between the saturated and the pure fluid (density jump at the beginning of the simulation). To determine the local value of the fluid density ρ^*, which is required to compute the buoyancy term in Eq. (2), we use the transport equation for the solute concentration C^*,

$$\phi \frac{\partial C^*}{\partial t^*} + u^* \frac{\partial C^*}{\partial x^*} + w^* \frac{\partial C^*}{\partial z^*} = \phi D \left(\frac{\partial^2 C^*}{\partial x^{*2}} + \frac{\partial^2 C^*}{\partial z^{*2}} \right), \tag{4}$$

in which D is solute diffusivity and t^* is time. We assume here that the diffusion coefficient is constant (see [37–39] for a detailed discussion of the effects of dispersion on the flow stability and on the dissolution process).

Dimensionless equations

The reference velocity scale for the present flow configuration is the free-fall buoyancy velocity $W^* = gk\Delta\rho_s^*/\mu$, which is the characteristic downward velocity of a dense fluid parcel immersed in a light fluid. We assume that the reference length scale is $\ell^* = \phi D/W^*$, defined as the length over which advection is balanced by diffusion. Variables are made dimensionless as follows [12,40,41]:

$$x = \frac{x^*}{\ell^*}, \quad z = \frac{z^*}{\ell^*}, \quad u = \frac{u^*}{W^*}, \quad w = \frac{w^*}{W^*}, \tag{5}$$

$$p = \frac{p^*}{\Delta\rho_s^* g \ell^*}, \quad C = \frac{C^*}{C_s^*}, \quad t = \frac{t^*}{\phi\ell^*/W^*}. \tag{6}$$

With reference to the dimensionless variables defined above, the governing balance equations become

$$\frac{\partial u}{\partial x} + \frac{\partial w}{\partial z} = 0, \tag{7}$$

$$u = -\frac{\partial P}{\partial x}, \quad w = -\frac{\partial P}{\partial z} - C, \tag{8}$$

$$\frac{\partial C}{\partial t} + u \frac{\partial C}{\partial x} + w \frac{\partial C}{\partial z} = \frac{\partial^2 C}{\partial x^2} + \frac{\partial^2 C}{\partial z^2}, \tag{9}$$

where $P = p + z(\rho_s^*/\Delta\rho_s^* - 1)$ is the reduced pressure. The governing parameter of the present system is the global (or final) Rayleigh-Darcy number Ra_0, defined as [40]

$$\mathrm{Ra}_0 = \frac{g\Delta\rho_s^* k H^*}{\mu \phi D} = \frac{H^*}{\ell^*}. \tag{10}$$

This dimensionless parameter represents the ratio of diffusive to convective timescales and contains information about the fluid properties ($\Delta\rho_s^*$, μ, and D), the porous medium properties (k and ϕ), and the domain size (H^*). We will simply refer to Ra_0 as the Rayleigh number hereinafter. Although
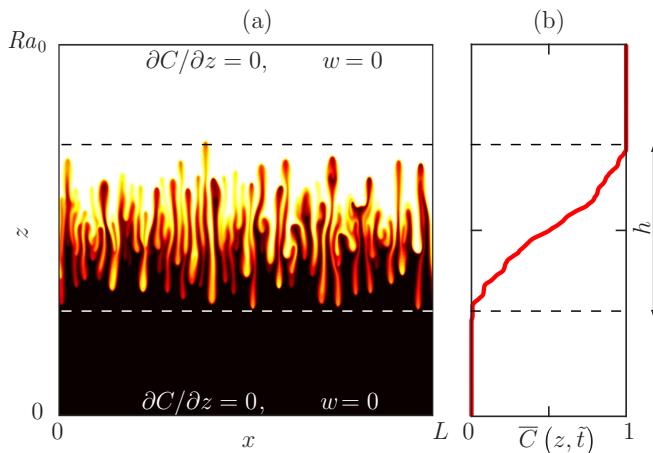
FIG. 1. (a) Sketch of the computational domain with explicit indication of the boundary conditions. The contour map of the solute concentration $C(x, z, \tilde{t})$ for a given time instant $t = \tilde{t}$ is also shown to provide a qualitative picture of the dynamics for the present physical configuration. (b) Horizontally averaged concentration profile $\overline{C}(z, \tilde{t})$ at the same time instant $\tilde{t}$ considered in (a). The instantaneous mixing length h is explicitly indicated as the extension of the tip-to-rear finger region (dashed lines).

not explicitly appearing in the governing equations (7)–(9), this parameter enters the picture as the dimensionless height of the domain.

Impermeable boundary conditions (i.e., no-flux conditions) for both fluid and solute are imposed at the top and bottom horizontal boundaries, whereas periodicity is applied at the side boundaries (along x). In dimensionless form, these boundary conditions become

$$w = 0, \quad \frac{\partial C}{\partial z} = 0 \quad \text{for} \quad z = 0, \quad z = \text{Ra}_0. \tag{11}$$

A key quantity that is usually introduced to describe the dynamics of RT instability is the mixing length h^* [5,27,42,43], which represents the average crest-to-throat distance of the deformed liquid-liquid interface. This quantity can be defined based on the local [43] (i.e., threshold) or global [44] (i.e., integral) value of the concentration field $C(x, z, t)$. Following De Wit [43], we identify the dimensionless mixing length h as the region where $\varepsilon < \overline{C}(z, t) < 1 - \varepsilon$, with $\overline{C}(z, t) = 1/L \int_0^L C(x, z, t)dx$ the concentration field averaged along the horizontal direction x, $\varepsilon = 10^{-2}$ a small tolerance parameter, and $L = L^*/\ell^*$ the dimensionless layer extension in the horizontal direction x. Further details on alternative definitions of the mixing length are provided in Sec. IV. Note that a local Rayleigh number (also called mixing, effective, or current Rayleigh number) can be defined using h^* (rather than H^*) as the reference length:

$$\text{Ra} = \frac{g\Delta\rho^* k h^*}{\mu\phi D} = \frac{h^*}{\ell^*} = h. \tag{12}$$

Values of the local Rayleigh number range between $0 \leqslant \text{Ra} \leqslant \text{Ra}_0$, with this parameter being conveniently introduced to compare systems that might be globally different, but locally similar, since they are characterized by the same extension of the mixing region (i.e., same h). A sketch of the computational domain is shown in Fig. 1(a) together with an instantaneous contour map of the concentration field at a given Ra_0 so as to give a flavor of the evolution of the flow [Fig. 1(a)] and of the flow parameters [Fig. 1(b)].

The governing equations (7)–(9) have been solved with a pseudospectral Chebyshev-Tau method employing a discrete Fourier transform in the horizontal direction and Chebyshev polynomials in the vertical direction [24,40,45]. We performed numerical simulations for different values of the

Rayleigh numbers Ra_0 in the range $10 \leqslant Ra_0 \leqslant 19\,953$. Starting from 10, Ra_0 was increased by a multiple factor of 10^a, with $a = 0.22$. Since we want to characterize the dynamics of the entire dissolution process in realistic conditions, in the following we will focus on large Ra_0 only (i.e., $Ra_0 > 3 \times 10^2$). All the simulations have been performed on a domain with $L = \pi/2$, with the exception of $Ra_0 = 19\,953$, which has been computed with $L = \pi/4$. The time step has been chosen to fulfill the Courant-Friedrichs-Lewy condition. For the largest Rayleigh number considered here ($Ra_0 = 19\,953$), we discretized the domain using 2048×1025 collocation points and adopting a time step $\Delta t = 1/2$.

III. RESULTS

In the following we will present and analyze the results obtained from an extensive campaign of numerical simulations of Rayleigh-Taylor convective dissolution in confined porous media, for different Rayleigh numbers in the range $347 \leqslant Ra_0 \leqslant 19\,953$.

A. Flow phenomenology

We start our discussion by looking at the qualitative evolution of the flow field. Results are shown for $Ra_0 = 12\,023$ only, since all the essential physical mechanisms we wish to discuss are clearly observable at this value of the Rayleigh number. The evolution of the flow field is faithfully rendered in Fig. 2 using contour maps of the concentration field C at different time instants, as explicitly indicated in the caption. The concentration field is initialized such that a heavier fluid layer (white layer in Fig. 2) lies on top of a lighter fluid layer (black layer in Fig. 2). Unstable modes are triggered by adding a random perturbation of the interface separating the two fluids, i.e., along $z = Ra_0/2$. The perturbation, characterized by an amplitude of 10^{-3}, is only applied at the first time instant ($t = 0$). After an initial stage dominated by diffusion [Fig. 2(a)], small fingers form at the interface [Fig. 2(b)] and start moving upward and downward in an almost symmetric fashion. Upon formation, fingers grow in time and interact, generating large ascending and descending plumes [Figs. 2(c)–2(e)] during a stage that, although dominated by convection, remains influenced by diffusion that drives the lateral spreading of the fingers' interface [5,14]. Under the vigorous action of buoyancy, plumes move predominantly in the vertical direction until they impinge on the boundaries where, due to the impermeability condition, they are forced to move laterally along the horizontal direction. At this stage, heavy fluid settles at the bottom of the domain, while light fluid accumulates at the top [Figs. 2(f)–2(h)]. This creates a stable density stratification that progressively hinders convection until the complete shutdown [Fig. 2(i)]. Naturally, the dynamics of fingers and plumes described above shares similarities with that observed for RB convection in porous media [20,21,24].

The evolution of the averaged concentration profile $\overline{C}(z/Ra_0, t)$ corresponding to the different flow instances discussed above is shown in Figs. 2(j)–2(l) as a function of the vertical coordinate z/Ra_0. In each of these three panels, the averaged profiles obtained from the three qualitative pictures displayed on the same row are shown. Note that overbars denote an average done in space and performed along the horizontal direction only.

As expected, shortly after perturbing the interface, the concentration profile follows closely the analytical profile of pure diffusion [see the mean profile in Fig. 2(j) corresponding to the qualitative picture in Fig. 2(a) taken at $t = 0.02 \times 10^4$]. As soon as fingers develop and grow, the concentration profile becomes more fluctuating. Upon impingement of plumes with the boundaries, concentration rises at the bottom and drops at the top [Fig. 2(f) taken at $t = 3.27 \times 10^4$, and the corresponding mean profile in Fig. 2(k)]. This marks the beginning of the shutdown phase, which is characterized by the progressive achievement of a completely stable density profile [Fig. 2(i) taken at $t = 1.34 \times 10^5$, and the corresponding mean profile in Fig. 2(l)]. In the long-term limit, a fully homogeneous concentration profile [$\overline{C}(z, t \to \infty) = 1/2$] is finally attained.

To characterize further the transient evolution of the flow, we focus on the time behavior of the dimensionless mixing length h normalized by the Rayleigh number Ra_0 and of the Sherwood number Sh (Fig. 3). The Sherwood number, which represents a dimensionless measure of the
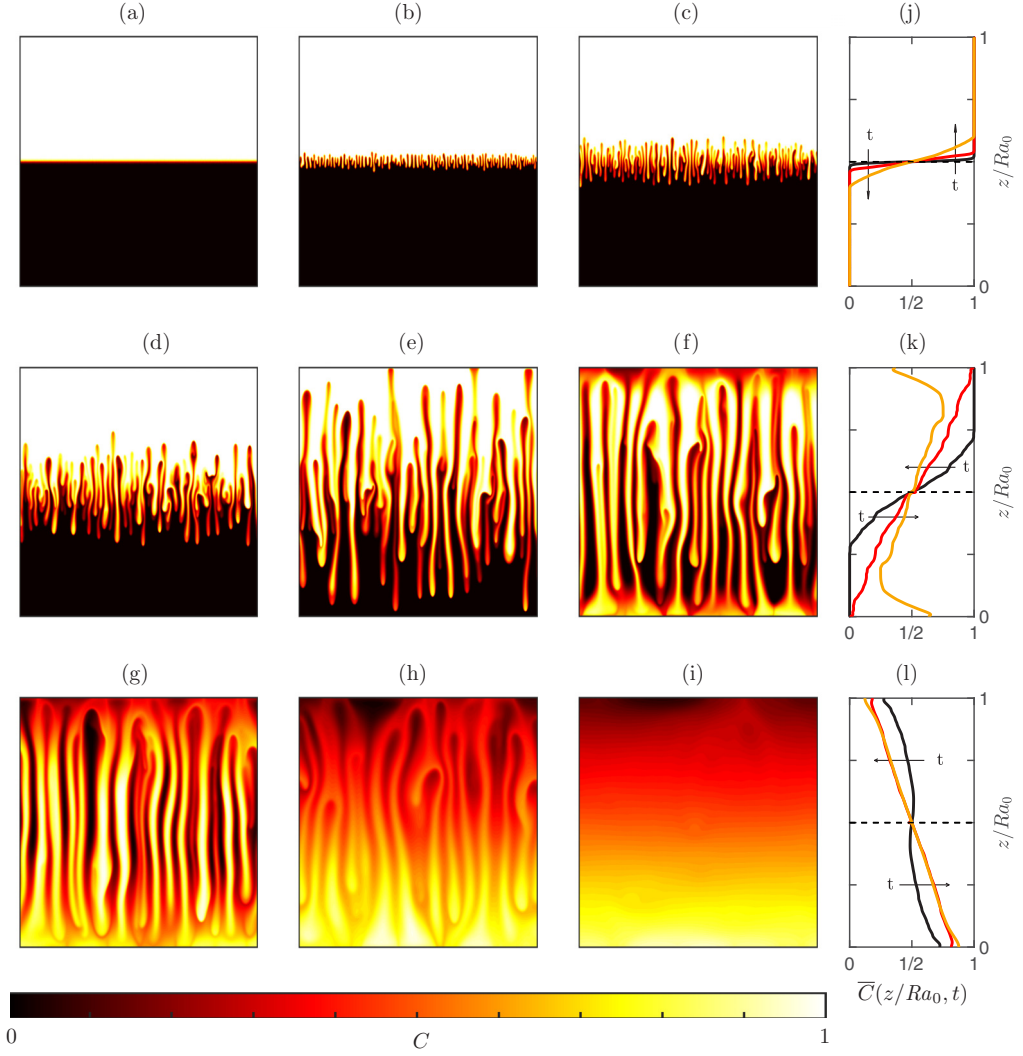
FIG. 2. (a)–(i) Snapshots of the concentration field for $Ra_0 = 12\,023$ at different time instants: (a) $t = 0.02 \times 10^4$, (b) $t = 0.29 \times 10^4$, (c) $t = 0.57 \times 10^4$, (d) $t = 1.11 \times 10^4$, (e) $t = 2.19 \times 10^4$, (f) $t = 3.27 \times 10^4$, (g) $t = 4.35 \times 10^4$, (h) $t = 6.53 \times 10^4$, and (i) $t = 1.34 \times 10^5$. Note that the aspect ratio of the cell has been modified here to $L/H = 1$ for visualization purposes only. (j)–(l) Instantaneous horizontally averaged concentration profiles corresponding to snapshots in a given row: (j) profiles from (a)–(c); (k) profiles from (d)–(f); and (l) profiles from (g)–(i).

dissolution efficiency, is defined as [20,27]

$$\mathrm{Sh} = \frac{\langle w^* C^* \rangle h^*}{\phi D C_s^*},\tag{13}$$

where angular brackets represent the average computed over the entire domain. The Sherwood number can be rewritten in terms of dimensionless variables as

$$\mathrm{Sh} = \langle wC \rangle \mathrm{Ra},\tag{14}$$
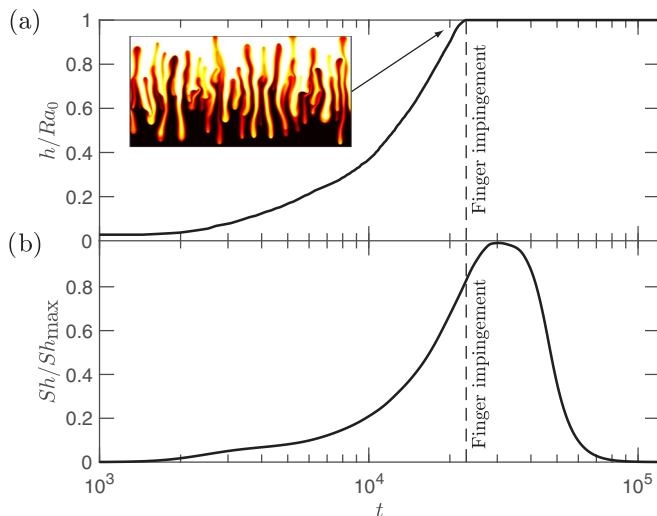
FIG. 3. Time evolution of (a) the normalized mixing length h/Ra_0 and (b) the normalized Sherwood number Sh/Sh_{max} for $\mathrm{Ra}_0 = 12\,023$. A vertical dashed line is drawn to indicate the time instant at which plumes impinge at the boundary. A contour map of the concentration distribution at this specific instant is also included for clarity.

with Ra the local Rayleigh number defined in Eq. (12). Sometimes the Sherwood number defined as in Eq. (13) is also called the mass-transfer Nusselt number. As expected, the mixing length [Fig. 3(a)] is a monotonic increasing function of time: The mixing process, which is initially slow and controlled by diffusion, becomes faster when dominated by convective fingers or plumes. Naturally, the mixing length has a maximum when plumes reach the boundaries (and this maximum corresponds to the domain height, i.e., $h/\mathrm{Ra}_0 = 1$). More detailed considerations of the time behavior of h will be given in Sec. III B.

During the initial diffusive stage, the Sherwood number remains approximately zero (solute convection is negligible). As soon as small fingers appear ($t \simeq 2 \times 10^3$), the Sherwood number increases, though remaining small in magnitude. During this stage, finger growth is linear and occurs predominantly in the vertical direction, with little or no lateral movement. After this initial linear growth, fingers become long enough so that their vertical motion turns out to be unstable and exhibits also lateral movements. At this stage ($t \simeq 5 \times 10^3$), fingers interact and merge into large plumes. Such a complex interaction promotes solute convection and induces a rapid increase of the Sherwood number. When large plumes reach the opposite boundary ($t \simeq 2.3 \times 10^4$), the Sherwood number is still increasing (see the dashed line indicating the first impact of a plume with the boundary). This happens because the main contribution to the Sherwood number comes from the core part of the domain (where momentum and energy transfer are higher), which is still not influenced by the presence of the boundaries. Upon impact of plumes with the boundaries, heavy (light) solute deposits at the bottom (top) boundary, hence hindering convection and mixing until the final complete shutdown.

B. Mixing length and Sherwood number: Analysis and modeling approaches

The temporal evolution of the mixing length for all the Rayleigh numbers considered in this study is presented in Fig. 4. The entire evolution of the mixing length h appears universal, in that its behavior is essentially independent of the value of the global Rayleigh number Ra_0 (whose value is explicitly indicated next to each curve). For $t < 10^3$, the process of solute transport is purely controlled by diffusion, and the behavior of the concentration C, obtained starting from the initial
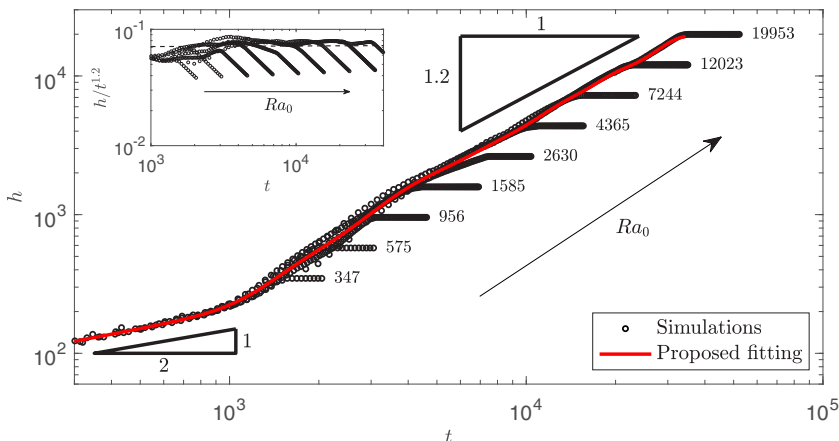
FIG. 4. Evolution in time of the mixing length h (symbols) for all the values of the global Rayleigh number Ra_0 (explicitly indicated next to each curve) considered in this study. The proposed fitting (red solid line) and the scaling laws (triangles) are also shown for comparison: During the diffusive stage $h \sim t^{1/2}$, whereas during the asymptotic nonlinear convective stage $h \sim t^{\alpha}$, with $\alpha = 1.208 \pm 0.008$ (superlinear scaling). To emphasize the proposed scaling law for the mixing length in the asymptotic nonlinear convective stage, a plot of $h/t^{1.2}$ is also shown in the inset.

stepwise profile, follows the analytical solution for the purely diffusive case

$$C(z,t) = \tfrac{1}{2}[1 + \mathrm{erf}(\psi)], \tag{15}$$

where $\psi = (z - Ra_0/2)/\sqrt{4t}$. The corresponding mixing length, computed as explained in Sec. II, becomes

$$h(t) = z_2 - z_1 = -2\sqrt{4t}\,\mathrm{erf}^{-1}(2\varepsilon - 1) \tag{16}$$

$$\approx \sqrt{4\pi}(1 - 2\varepsilon)\sqrt{t} \sim \sqrt{t}. \tag{17}$$

This theoretical behavior fits nicely the results of the numerical simulations during the initial stage (see Fig. 4). A similar trend was recently observed by Gopalakrishnan et al. [5] in the same flow configuration analyzed here. This trend was also recovered for the case of RT instability in pure fluids and assuming different initial conditions by Biferale et al. [46].

After the initial stage dominated by diffusion, perturbations grow and the flow enters a long stage dominated by convection and characterized by the appearance and corresponding development of fingers (see also the description of the flow phenomenology provided in Sec. III A). A trend based on data fitting has been proposed by Gopalakrishnan et al. [5], who found a linear scaling for the growth of the mixing length in the convective stage. In this work, we are also able to come to a more precise estimate of this scaling. We notice that the asymptotic behavior of the mixing length (i.e., the behavior for $t > 10^4$, which can be attained only for $Ra_0 > 4 \times 10^3$) is apparently universal but superlinear, being approximated by the power law $h \sim t^{\alpha}$, with $\alpha = 1.208 \pm 0.008$. Therefore, to emphasize the robustness of the proposed scaling in the nonlinear convective stage, we compute the quantity $h/t^{1.2}$. Results are shown in the inset of Fig. 4. As expected, the rescaled mixing length $h/t^{1.2}$ relaxes onto an horizontal plateau, clearly indicating the attainment of such an asymptotic regime. We have extensively tested the proposed scaling also changing the aspect ratio of the domain in the range $\pi/4 \leqslant L/Ra_0 \leqslant \pi/2$ to be sure that this result is not influenced by the domain size [47]. Note that there is an elusive region between the initial diffusion-dominated stage and the final convection-dominated stage ($10^3 < t < 10^4$), during which the behavior of h slightly depends on the value of Ra_0 and cannot be easily parametrized.
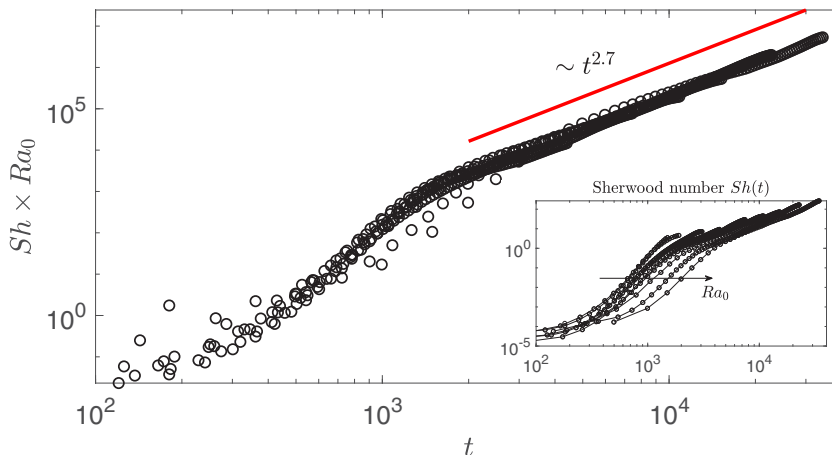
FIG. 5. Evolution in time of the Sherwood number rescaled as $Sh \times Ra_0$ (symbols) for all the values of the global Rayleigh number Ra_0 considered in this study. Results are shown up to the instant at which the fastest plume impinges on the boundary. The proposed scaling $Sh \times Ra_0 \sim t^{2.7}$ is also shown for comparison. In the inset, we also show the behavior in time of the Sherwood number Sh, i.e., without the rescaling factor Ra_0.

In Fig. 5 we focus on the behavior of the Sherwood number Sh: In the inset we show the evolution of Sh in time for all the values of the global Rayleigh number Ra_0 considered here ($347 \leqslant Ra_0 \leqslant 19\,953$), whereas in the main panel we show the behavior in time of the Sherwood number rescaled as $Sh \times Ra_0$. All the results in this picture are shown up to the time instant at which the faster plume reaches the boundary, so as to exclude from the analysis the shutdown phase, during which Sh inevitably drops. As already discussed in Fig. 3, for a given value of Ra_0, Sh increases monotonically in time. While the increase of Sh is slow at the beginning, when the flow is controlled by diffusion, it becomes faster when the flow is dominated by convection. When properly rescaled as $Sh \times Ra_0$, all results collapse and follow the unified asymptotic behavior $Sh \times Ra_0 \sim t^{2.7}$. We believe that such a prediction could be helpful for future parametrization of transport processes in the present configuration.

C. Wall-induced convective shutdown

In almost all the flow transport instances of practical importance in environmental and industrial applications, the presence of boundaries plays a crucial role [12,48]. Despite this, the presence of boundaries is usually neglected in the framework of the RT instability and the flow dynamics is analyzed only up to the point at which flow structures reach the limit of the computational domain in the vertical direction. There are only a few works [5,29] on RT instability in confined porous media, which however mainly focused on the role of chemical reactions at the fluid-fluid interface, or on the relative role of diffusion and convection during the initial flow evolution (i.e., ruling out the shutdown phase occurring after plume impingement).

Here we quantify the effect of the vertical confinement by computing the time t_t required for rising (falling) fingers to impinge on the top (bottom) boundary. In particular, we define t_t as

$$t_t \, \forall t \geqslant t_t, \quad h(t)/Ra_0 \geqslant 1 - \varepsilon, \tag{18}$$

with $\varepsilon = 10^{-2}$. In other words, at time larger that t_t, the normalized distance of the average finger tip from the wall is smaller than ε. As apparent from Fig. 6, the behavior of t_t as a function of the Rayleigh number Ra_0 (in the range of moderate to large Rayleigh numbers) is well described by the power law $t_t = 14.98 \times Ra_0^{0.78}$. This reflects the physical intuition that the time a plume takes to reach the boundary is increasing with Ra_0, i.e., with the domain height. However, the increase is
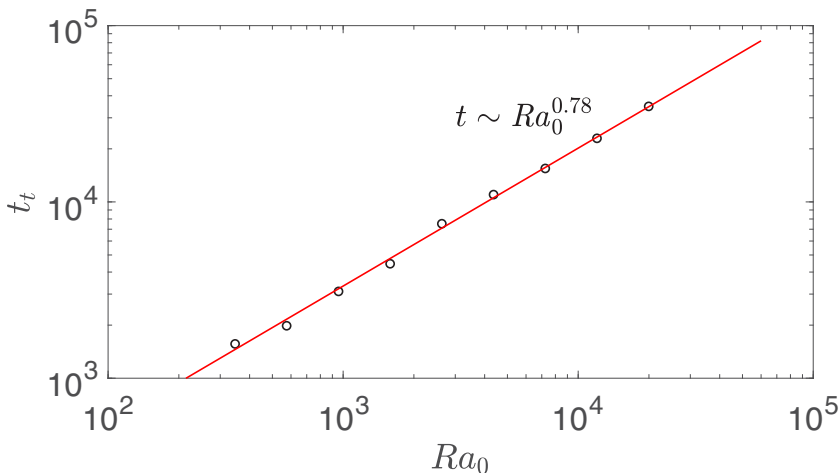
FIG. 6. Time taken by fingers to reach the horizontal boundaries (t_t) as a function of Ra_0 for simulations in the range $347 \leqslant Ra_0 \leqslant 19\,953$. The proposed fitting $14.98 \times Ra_0^{0.78}$ is also explicitly shown.

lower than the expected linear increase that would occur in the case of a simple rising and falling plume in pure fluids moving at constant (buoyancy) velocity, hence indicating a vertical plume acceleration. This behavior is possibly due to the complex nonlinear interaction among plumes that characterizes the entire mixing process and hinders the application of simplified considerations to parametrize it. After plumes impinge on the boundaries, convection becomes gradually less important compared to diffusion and the system enters the shutdown phase, with the concentration distribution slowly attaining an equilibrium (and stable) profile characterized by a perfectly mixed solute.

IV. PHENOMENOLOGICAL MODEL FOR THE TIME EVOLUTION OF MIXING LENGTH

In this section we propose a simplified phenomenological model to estimate the amount of mixing induced by RT instability in a porous medium. Such an estimate is of specific importance to design industrial equipments employing porous material or to analyze environmental and geophysical processes.

Since there is no model available to predict the mixing process for RT configuration in porous media, we took inspiration from the models mostly developed for turbulent flows. A comprehensive review of this topic was recently offered by Boffetta and Mazzino [27].

The model we present in this section is inspired by the work of Cook *et al.* [44], who described the growth of the mixing region during RT instability in pure fluids. This model is based on the evaluation of the mass fluxes across an horizontal surface located at a specific height $z = z_0$ at which the value of the mean concentration is $\overline{C}(z_0, t) = 1/2$. Due to the symmetry of our system, and considering also the boundary conditions (impermeable walls, i.e., closed system) and the initial condition (upper and lower half of the domain characterized by $C = 1$ and by $C = 0$, respectively), we have $z_0 = Ra_0 /2$. To identify properly the mixing region, we conveniently rescale the concentration profile as

$$C_r(C) = 1 - 2|\overline{C} - 1/2| \tag{19}$$

so as to have $C_r = 1$ when both fluids are mixed in equal proportion ($\rho^* = \rho_s^* - \Delta\rho_s^*/2$) and $C_r = 0$ when only one fluid is present ($\rho^* = \rho_s^*$ or $\rho^* = \rho_s^* - \Delta\rho_s^*$). The behavior of C and C_r with the fluid density is shown in Fig. 7(a). When plotted as a function of the vertical position z/Ra_0, the actual ($\overline{C}$) and the rescaled (C_r) mean concentrations behave as shown in Fig. 7(b). As already mentioned in
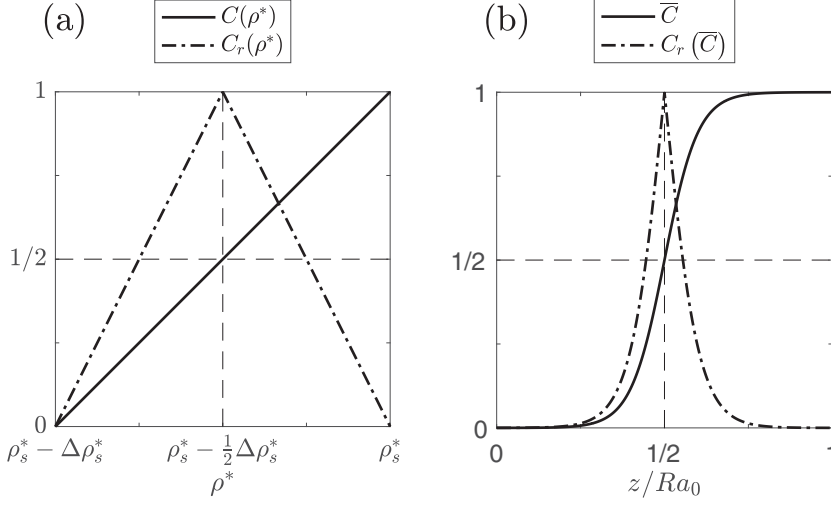
FIG. 7. (a) Dimensionless concentration C (solid line) and rescaled concentration C_r (dash-dotted line) represented as a function of the local density ρ^*. Due to the definition adopted in (19), the value of C_r is maximum for $\overline{C} = 1/2$ and minimum when $\overline{C} = 0$ or $\overline{C} = 1$. (b) Example of rescaled concentration field C_r plotted as a function of the average concentration field $\overline{C}(z)$.

Sec. II, different definitions are available to quantify the mixing length h that measures the extension of the mixing region. Here we follow Cook *et al.* [44] and we define the mixing length as

$$h = \alpha \int_0^{\mathrm{Ra}_0} C_r(z)dz. \tag{20}$$

The use of this latter definition for h, which gives the same results compared to the definition of h introduced in Sec. II and based on the identification of a threshold value, is however more suitable to derive theoretical models based on analytical approaches. Nice agreement between the results obtained by the two different definitions of h is reached upon introduction of the factor $\alpha = 9.3$ in Eq. (20). Assuming that the mean concentration profile is symmetric with respect to $z_0 = \mathrm{Ra}_0 /2$, and using the definition (19), Eq. (20) becomes

$$h = 2\alpha \int_{\mathrm{Ra}_0 /2}^{\mathrm{Ra}_0} [1 - 2\overline{C}(z)]dz. \tag{21}$$

Mass conservation for incompressible miscible fluids immersed in homogeneous and isotropic porous media reads [49]

$$\phi \frac{\partial \rho^*}{\partial t^*} + \frac{\partial (\rho^* u^*)}{\partial x^*} + \frac{\partial (\rho^* w^*)}{\partial z^*} = 0. \tag{22}$$

Assuming that the flow is periodic along x and that $\overline{u^*} = \overline{w^*} = 0$ (i.e., no mean flow along x and z), Eq. (22), averaged along x and complemented by Eq. (3), becomes

$$\frac{\partial \overline{C}}{\partial t} + \frac{\partial \overline{Cw}}{\partial z} = 0. \tag{23}$$

The time derivative of Eq. (21), written using also Eq. (23), gives

$$\frac{\partial h}{\partial t} = -4\alpha \overline{Cw}(z_0). \tag{24}$$
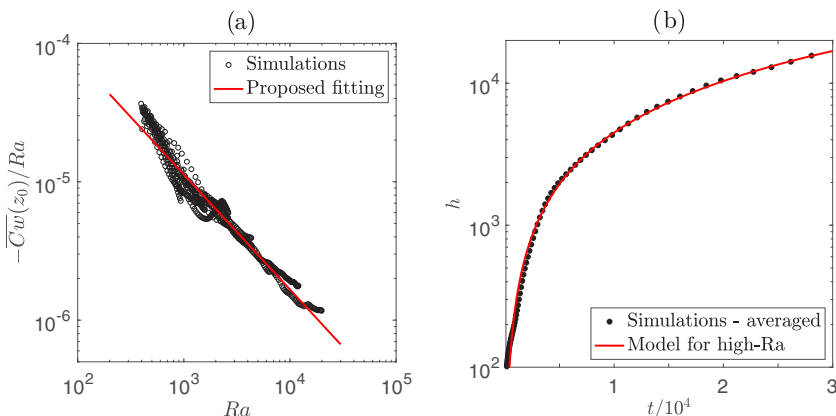
FIG. 8. (a) Behavior of the correlation $-\overline{Cw}$ as a function of the local Rayleigh number Ra for different simulations in the range $347 \leqslant \mathrm{Ra}_0 \leqslant 19\,953$ (open circles). The proposed fitting [red solid line, Eq. (25)] of $-\overline{Cw}$ is also explicitly shown. (b) Comparison between the averaged behavior of h computed from the entire numerical database (closed circles) and the prediction of the phenomenological model [Eq. (26)].

This equation, which expresses the time variation of the mixing length h, is valid for both confined and unconfined porous media in the vertical direction, provided $\overline{C}(z_0) = 1/2$.

At this stage, to obtain the explicit behavior of $h(t)$ we introduce a proper parametrization for $\overline{Cw}$. From the analysis of our numerical database, we observe that the correlation $\overline{Cw}$, when properly rescaled, exhibits a rather robust behavior [Fig. 8(a)] that can be conveniently parametrized. In particular, we observe that

$$-\overline{Cw}(z_0) \approx \beta \, \mathrm{Ra}^\gamma, \tag{25}$$

where β and γ are two model constants that are introduced to reproduce faithfully the numerical results. Based on our computation, we get $\gamma = 0.169 \pm 0.014$ and $\beta = 0.0035 \pm 0.0004$.

Using the correlation (25), and considering that $\mathrm{Ra} = h$, the integral of Eq. (24) with the initial condition $h(t_0) = t_0 = 0$ gives

$$h = \delta t^{1/(1-\gamma)}, \tag{26}$$

where $\delta = [4\alpha\beta(1-\gamma)]^{1/(1-\gamma)} = 0.0687$. Note that the value of the exponent that characterizes the growth of h with time t, i.e., $1/(1-\gamma) = 1.204$, is in good agreement with that observed in the numerical simulations, 1.208 (see Fig. 4 and the corresponding description). The explicit comparison of the time behavior of $h = f(t)$ is shown in Fig. 8(b). Symbols are obtained by averaging all the numerical results for $\mathrm{Ra}_0 \geqslant 347$ (a value that we took as a threshold to indicate the beginning of a convection-dominated regime). As expected, the agreement between the prediction given by the model [red line in Fig. 8(b)] and the numerical simulations [symbols in Fig. 8(b)] is satisfactory. This is partially due to the construction of the model, which used some of the simulations data, but indicates also the robustness of the employed modeling strategy and hypotheses. We wish also to remark here that the growth rate of h with time t is close to the linear behavior estimated in previous studies [5]. Yet it is superlinear, a result that makes the growth of the mixing length faster than expected.

V. CONCLUSION

In this work, numerical simulations were used to analyze the evolution of solute convection driven by Rayleigh-Taylor instability in isotropic and homogeneous vertically confined porous media. We performed an extensive campaign of pseudospectral numerical simulations for different

values of the Rayleigh number Ra_0 in the range $347 \leqslant Ra_0 \leqslant 19\,953$. The initial condition of each simulation consists of a layer of heavy fluid sitting on top of a layer of light fluid. The time-dependent dynamics of the flow is characterized by the appearance of three consecutive main stages: At the beginning, the process of solute transport at the liquid-liquid interface is dominated by diffusion; later, small fingers appear at the interface, grow in time, and merge to form larger plumes during a stage dominated by convection. Finally, plumes reach the boundaries and the flow enters a shutdown stage. The entire transient dynamics described above has been carefully characterized, focusing in particular on the evolution of the mixing length h, a quantity used to measure the extension of the mixing region. During the initial diffusive stage, the mixing length evolves as $h \sim t^{1/2}$. After the diffusive stage, the flow enters a convection-dominated stage that is ultimately characterized by an asymptotic superlinear behavior of the mixing length. With our results, we confirm the qualitative trend found in previous numerical and experimental studies [5], but we also evaluate precisely the value of the exponent to be $h \sim t^{1.2}$. Based on the original results of the present computations, we have also developed a simplified phenomenological model to predict the time evolution of the mixing length in RT instability in porous media.

Although experiments, simulations, and theoretical analysis have provided plentiful data on the dynamics of viscosity and gravity-driven flows in porous media, the field remains rich in future challenges. One important aspect that in our opinion requires further attention is the inclusion of chemical reactions taking place during the mixing process between the two fluids. Chemical reactions usually occur at the interface separating the two fluids and can trigger or suppress fluid instabilities. This issue was recently studied for the case of miscible fluids [29] and should be also studied for the case of partially miscible [30,50,51] or immiscible fluids [52].

---

[1] Lord Rayleigh, Investigation of the character of the equilibrium of an incompressible heavy fluid of variable density, Proc. London Math. Soc. **s1–14**, 170 (1882).

[2] G. I. Taylor, The instability of liquid surfaces when accelerated in a direction perpendicular to their planes. I, Proc. R. Soc. London Ser. A **201**, 192 (1950).

[3] P. G. Saffman and G. Taylor, The penetration of a fluid into a porous medium or Hele-Shaw cell containing a more viscous liquid, Proc. R. Soc. London Ser. A **245**, 312 (1958).

[4] G. M. Homsy, Viscous fingering in porous media, Annu. Rev. Fluid Mech. **19**, 271 (1987).

[5] S. S. Gopalakrishnan, J. Carballido-Landeira, A. De Wit, and B. Knaepen, Relative role of convective and diffusive mixing in the miscible Rayleigh-Taylor instability in porous media, Phys. Rev. Fluids **2**, 012501 (2017).

[6] S. Backhaus, K. Turitsyn, and R. Ecke, Convective Instability and Mass Transport of Diffusion Layers in a Hele-Shaw Geometry, Phys. Rev. Lett. **106**, 104501 (2011).

[7] L. Paterson, Radial fingering in a Hele-Shaw cell, J. Fluid Mech. **113**, 513 (1981).

[8] J.-D. Chen and D. Wilkinson, Pore-Scale Viscous Fingering in Porous Media, Phys. Rev. Lett. **55**, 1892 (1985).

[9] L. Paterson, Diffusion-Limited Aggregation and Two-Fluid Displacements in Porous Media, Phys. Rev. Lett. **52**, 1621 (1984).

[10] R. A. Wooding, Growth of fingers at an unstable diffusing interface in a porous medium or Hele-Shaw cell, J. Fluid Mech. **39**, 477 (1969).

[11] J. Fernandez, P. Kurowski, P. Petitjeans, and E. Meiburg, Density-driven unstable flows of miscible fluids in a Hele-Shaw cell, J. Fluid Mech. **451**, 239 (2002).

[12] A. C. Slim, Solutal-convection regimes in a two-dimensional porous medium, J. Fluid Mech. **741**, 461 (2014).

[13] P. Jenny, J. S. Lee, D. W. Meyer, and H. A. Tchelepi, Scale analysis of miscible density-driven convection in porous media, J. Fluid Mech. **749**, 519 (2014).

[14] J. A. Neufeld, M. A. Hesse, A. Riaz, M. A. Hallworth, H. A. Tchelepi, and H. E. Huppert, Convective dissolution of carbon dioxide in saline aquifers, Geophys. Res. Lett. **37**, L22404 (2010).

[15] M. Mishra, M. Martin, and A. De Wit, Differences in miscible viscous fingering of finite width slices with positive or negative log-mobility ratio, Phys. Rev. E **78**, 066306 (2008).

[16] O. K. Matar and S. M. Troian, Spreading of a surfactant monolayer on a thin liquid film: Onset and evolution of digitated structures, Chaos **9**, 141 (1999).

[17] H. E. Huppert and J. A. Neufeld, The fluid mechanics of carbon dioxide sequestration, Annu. Rev. Fluid Mech. **46**, 255 (2014).

[18] A. Riaz and Y. Cinar, Carbon dioxide sequestration in saline formations: Part I—Review of the modeling of solubility trapping, J. Petrol. Sci. Eng. **124**, 367 (2014).

[19] H. Emami-Meybodi, H. Hassanzadeh, C. P. Green, and J. Ennis-King, Convective dissolution of CO_2 in saline aquifers: Progress in modeling and experiments, Int. J. Greenhouse Gas Control **40**, 238 (2015).

[20] J. Otero, L. A. Dontcheva, H. Johnston, R. A. Worthing, A. Kurganov, G. Petrova, and C. R. Doering, High-Rayleigh number convection in a fluid-saturated porous layer, J. Fluid Mech. **500**, 263 (2004).

[21] D. R. Hewitt, J. A. Neufeld, and J. R. Lister, Ultimate Regime of High Rayleigh Number Convection in a Porous Medium, Phys. Rev. Lett. **108**, 224503 (2012).

[22] B. Wen, L. T. Corson, and G. P. Chini, Structure and stability of steady porous medium convection at large Rayleigh number, J. Fluid Mech. **772**, 197 (2015).

[23] H. Emami-Meybodi and H. Hassanzadeh, Two-phase convective mixing under a buoyant plume of CO_2 in deep saline aquifers, Adv. Water Resour. **76**, 55 (2015).

[24] M. De Paoli, F. Zonta, and A. Soldati, Influence of anisotropic permeability on convection in porous media: Implications for geological CO_2 sequestration, Phys. Fluids **28**, 056601 (2016).

[25] M. R. Soltanian, M. A. Amooie, Z. Dai, D. Cole, and J. Moortgat, Critical dynamics of gravito-convective mixing in geological carbon sequestration, Sci. Rep. **6**, 35921 (2016).

[26] M. A. Amooie, M. R. Soltanian, and J. Moortgat, Solutal convection in porous media: Comparison between boundary conditions of constant concentration and constant flux, Phys. Rev. E **98**, 033118 (2018).

[27] G. Boffetta and A. Mazzino, Incompressible Rayleigh-Taylor turbulence, Annu. Rev. Fluid Mech. **49**, 119 (2017).

[28] T. Suekane, J. Ono, A. Hyodo, and Y. Nagatsu, Three-dimensional viscous fingering of miscible fluids in porous media, Phys. Rev. Fluids **2**, 103902 (2017).

[29] J. J. Hidalgo, M. Dentz, Y. Cabeza, and J. Carrera, Dissolution patterns and mixing dynamics in unstable reactive flow, Geophys. Res. Lett. **42**, 6357 (2015).

[30] V. Loodts, C. Thomas, L. Rongy, and A. De Wit, Control of Convective Dissolution by Chemical Reactions: General Classification and Application to CO_2 Dissolution in Reactive Aqueous Solutions, Phys. Rev. Lett. **113**, 114501 (2014).

[31] A. De Wit, Fingering of Chemical Fronts in Porous Media, Phys. Rev. Lett. **87**, 054502 (2001).

[32] C. Almarcha, P. M. J. Trevelyan, P. Grosfils, and A. De Wit, Chemically Driven Hydrodynamic Instabilities, Phys. Rev. Lett. **104**, 044501 (2010).

[33] S. Pramanik and M. Mishra, Stability of miscible Rayleigh-Taylor fingers in porous media with non-monotonic density profiles (unpublished).

[34] J. Martin, N. Rakotomalala, and D. Salin, Gravitational instability of miscible fluids in a Hele-Shaw cell, Phys. Fluids **14**, 902 (2002).

[35] A. J. Landman and R. J. Schotting, Heat and brine transport in porous media: The Oberbeck-Boussinesq approximation revisited, Transp. Porous Media **70**, 355 (2007).

[36] P. C. Myint and A. Firoozabadi, Onset of convection with fluid compressibility and interface movement, Phys. Fluids **25**, 094105 (2013).

[37] L. Wang, Y. Nakanishi, A. Hyodo, and T. Suekane, Three-dimensional structure of natural convection in a porous medium: Effect of dispersion on finger structure, Int. J. Greenhouse Gas Control **53**, 274 (2016).

[38] Y. Liang, B. Wen, M. A. Hesse, and D. DiCarlo, Effect of dispersion on solutal convection in porous media, Geophys. Res. Lett. **45**, 9690 (2018).

[39] H. Emami-Meybodi, Dispersion-driven instability of mixed convective flow in porous media, Phys. Fluids **29**, 094102 (2017).

[40] M. De Paoli, F. Zonta, and A. Soldati, Dissolution in anisotropic porous media: Modelling convection regimes from onset to shutdown, Phys. Fluids **29**, 026601 (2017).

[41] P. Cheng, M. Bestehorn, and A. Firoozabadi, Effect of permeability anisotropy on buoyancy-driven flow for CO_2 sequestration in saline aquifers, Water Resour. Res. **48**, W09539 (2012).

[42] S. Dalziel, P. Linden, and D. Youngs, Self-similarity and internal structure of turbulence induced by Rayleigh-Taylor instability, J. Fluid Mech. **399**, 1 (1999).

[43] A. De Wit, Miscible density fingering of chemical fronts in porous media: Nonlinear simulations, Phys. Fluids **16**, 163 (2004).

[44] A. W. Cook, W. Cabot, and P. L. Miller, The mixing transition in Rayleigh-Taylor instability, J. Fluid Mech. **511**, 333 (2004).

[45] F. Zonta, C. Marchioli, and A. Soldati, Modulation of turbulence in forced convection by temperature-dependent viscosity, J. Fluid Mech. **697**, 150 (2012).

[46] L. Biferale, G. Boffetta, A. A. Mailybaev, and A. Scagliarini, Rayleigh-Taylor turbulence with singular nonuniform initial conditions, Phys. Rev. Fluids **3**, 092601 (2018).

[47] B. Wen, G. P. Chini, N. Dianati, and C. R. Doering, Computational approaches to aspect-ratio-dependent upper bounds and heat flux in porous medium convection, Phys. Lett. A **377**, 2931 (2013).

[48] Y. Nakanishi, A. Hyodo, L. Wang, and T. Suekane, Experimental study of 3D Rayleigh-Taylor convection between miscible fluids in a porous medium, Adv. Water Resour. **97**, 224 (2016).

[49] D. Nield and B. Adrian, *Convection in Porous Media* (Springer, Berlin, 2006), Vol. 3.

[50] X. Fu, L. Cueto-Felgueroso, and R. Juanes, Viscous fingering with partially miscible fluids, Phys. Rev. Fluids **2**, 104001 (2017).

[51] V. Loodts, L. Rongy, and A. De Wit, Chemical control of dissolution-driven convection in partially miscible systems: Theoretical classification, Phys. Chem. Chem. Phys. **17**, 29814 (2015).

[52] L. Dedè, H. Garcke, and K. F. Lam, A Hele-Shaw-Cahn-Hilliard model for incompressible two-phase flows with different densities, J. Math. Fluid Mech. **20**, 531 (2018).